ForamJ – A Tool for the Reproducible, Semi-automated Analysis of Foraminifera Micro Computed Tomography Datasets

Jacob Trend[1], Fernando Alvarez Borges[2], Tali L. Babila[3],

1. School of Ocean and Earth Sciences, National Oceanographic Centre, University of Southampton, Southampton, SO14 3ZH, United Kingdom.
2. μ-VIS X-ray Imaging Centre, University of Southampton, Southampton, SO17 1BJ.
3. Department of Earth, Environmental, and Planetary Sciences, Case Western Reserve University, Cleveland, 44106, United States of America.

Abstract

The application of micro-computed tomography (μCT) to foraminiferal test analysis has opened new avenues for high-resolution, non-destructive 3D characterisation of internal and external morphological features. However, existing workflows are typically limited by low throughput, manual segmentation, and reliance on proprietary software, constraining dataset reproducibility and scalability. Here we present ForamJ, an open-source ImageJ plugin developed specifically for the semi-automated, reproducible analysis of foraminiferal μCT datasets. ForamJ streamlines key stages of image processing, including test segmentation, homogenous infill removal, chamber isolation, and morphological quantification, with outputs tailored to established micropaleontological metrics while providing a significant decrease in processing time versus existing methods. These include both calcite volume and chamber volumes, test surface area, inner and outer wall thickness, chamber centroid coordinates - parameters directly relevant to taxonomy, taphonomy, paleoecology, and biomineralisation processes. The plugin supports both single-sample and batch-processing workflows, enabling high-throughput analysis. Two use cases are presented: (1) the assessment of species-specific morphological variability in ancient cosmopolitan benthic foraminifera genus *Cibicidoides* spp. and (2) quantification of trends in between multiple species of modern planktonic foraminifera. Validation against manual segmentation of benthic foraminifera performed in commercial software ORS Dragonfly demonstrates ForamJ's analytical fidelity, with a 1.30% difference in calcite volume between ForamJ and manually annotated tests, with a 0.9981% (± 0.001) segmentation accuracy and 0.97 (± 0.008) dice score with a median processing speed of 154 seconds per sample. By embedding foraminifera-specific metrics into an accessible, reproducible, and extensible framework, ForamJ provides a lightweight, dedicated digital toolset for advancing μCT-based test analysis in foraminiferal research.

Keywords: Foraminifera, Micro Computed Tomography, Image Analysis, Workflow Development.

Corresponding author: Dr Jacob Trend, Jjt1f23@soton.ac.uk

Preprint statement: ***This paper is a non-peer reviewed preprint submitted to EarthArXiv. At the time of posting to EarthArXiv, it is currently being peer reviewed by Scientific Reports for publication.***

Introduction

Micro-computed tomography (µCT) is a widely used 3D imaging technique across disciplines such as life sciences (Papazoglou et al. 2021; Trend et al. 2023; Evans et al. 2024), geosciences (Cnudde and Boone 2013), materials science (Withers et al. 2021), and paleontology (Barker et al. 2023). Its key strength lies in its ability to provide high-resolution, three-dimensional, non-destructive visualisation of internal structures from a single scan. This generates rich volumetric datasets, often necessitating the development of tailored image analysis pipelines to extract meaningful, quantitative information.

One promising application of µCT is for the study of foraminifera; unicellular, sub-millimetre-sized, shelled amoeboid protists. Foraminifera are a predominantly marine group, inhabiting sediments on the seafloor (benthic) and within the upper ocean's water column (planktonic). Foraminifera produce multi-chambered calcium carbonate shells, or tests, whose morphology varies significantly between species and can reflect the climatic and environmental conditions in which calcification occurred (Kucera et al. 2005; Katz et al. 2010). Upon death, these tests are deposited and accumulated in seafloor marine sediments, where they can be preserved for millions of years, forming an extensive geologic archive for paleoenvironmental and paleoclimatic reconstructions (Westerhold et al. 2020; Judd et al. 2022).

µCT enables detailed imaging of both external test morphology (Kuroyanagi et al. 2021; Kinoshita et al. 2022; Zarkogiannis et al. 2025; Burke et al. 2020) and internal chamber architecture (Burke et al. 2020; Speijer et al. 2008; Burke et al. 2025; Duan et al. 2021; Briguglio et al. 2011; Lin et al. 2024), providing insights into taxonomy, taphonomy, growth patterns, and environmental responses. However, challenges arise due to intra-species morphological variability, the need for statistically robust sample sizes, and post-mortem alterations such as chamber wall dissolution and infilling, which complicate the segmentation processing and therein interpretation of original versus postmortem morphological features. These factors often necessitate manual input, reducing throughput and reproducibility. Therefore, to date, µCT imaging in foraminifera studies are generally limited in their test morphology parameterisation and sample size dataset. Thus, there is a need for image analysis tools to be optimised to handle large datasets and to accommodate for morphological variation between specimens. This must be paired with accurate, quantitative outputs, while minimising highly time-consuming and specialised imaging training required for manual segmentation.

Existing commercial image analysis software - such as ORS Dragonfly (Comet Technologies Canada Inc.), Avizo (Thermo Fisher Scientific Avizo), VG Studio (Volume Graphics GmbH) and IPSDK (IPSDK Explorer, Reactiv'IP) - are widely used for µCT segmentation, but are proprietary and to our knowledge, do not provide workflows specifically optimised for foraminiferal morphology, batch processing, and standardised chamber-level quantification. Several independent workflows for foraminiferal µCT analysis have been developed in the literature, including recent artificial intelligence (AI)–based approaches using annotated datasets to train deep learning pipelines, automating test and chamber segmentation (Mulqueeney et al. 2024). In parallel, continued advances in interactive and GUI-based frameworks for 3D biological imaging have lowered technical barriers for non-specialist users (Ma et al. 2024; Isensee et al. 2025). However, AI–based workflows typically still require manually annotated training data, model configuration, and computational resources, which can limit accessibility and reproducibility in foraminiferal studies. Individual studies have also began to address issues presented by foraminifera samples, such as chamber-to-chamber merging as a result of septal dissolution (He et al. 2025), and the development of specific quantitative parameters such as chamber trochospirality (Brombacher et al. 2022). However, an integrated workflow combining segmentation with downstream extraction of phenotypically relevant parameters for foraminiferal analysis is currently lacking.

To address this gap, we developed an open-source plugin for use within the ImageJ environment suite (Schindelin et al. 2012), enabling a streamlined, reproducible and self-guided workflow for µCT analyses of foraminifera. While ImageJ supports a range of domain-specific plugins, for example, in bone biology (Doube et al. 2010), neuroscience (Meijering et al. 2004; Arshadi et al. 2021) and ecology (Moore et al. 2013). However, no such tool currently exists for foraminiferal research. Our plugin –

ForamJ - aims to provide the foraminiferal research community with a dedicated, accessible solution for the quantitative analysis of µCT datasets.

Approach

The primary goal of this plugin is to provide an accessible and reproducible image analysis workflow tailored to the foraminiferal research community. A significant barrier to wider adoption of µCT-based analysis in this field is the reliance on commercial software, which often requires access to high-performance imaging workstations and specialised training. Even when such infrastructure is available, method development can be time-consuming, user dependent and inconsistent across labs. Furthermore, study of foraminifera often requires large sample sets to adequately characterise intra- and inter-population morphological variability high sample numbers and as such, a key aim was to make it scalable for larger datasets

To address these limitations, the plugin was designed with the following core principles:

1. **Accessibility** – It must be intuitive and usable by researchers with beginner level image analysis experience.
2. **Portability** – It must be able to run on standard, non-specialist computing hardware.
3. **Open Source** – It must function entirely within the open-source ImageJ ecosystem.
4. **Reproducibility** – It must produce standardised, quantitative outputs in a consistent and easily interpretable format.
5. **High throughput** – The plugin must provide a significant improvement in processing speed, with potential for batch processing.

To meet these criteria, we implemented a set of morphological measurements targeting both whole test and internal chamber architecture, based on established metrics described in the literature (Table 1). These measurements were selected to maximise biological relevance while ensuring they could be extracted reliably from typical µCT datasets, despite the presence of sediment infill, poor preservation and variable contrast between individuals. These factors may lead users to resist a one-size-fits-all approach to image segmentation (Figure 1) or necessitate a complex - and often inaccessible to new users - machine learning or deep learning-based solution to account for this variability. During the development of ForamJ, it was noted that the specimens that were used for the development of this plugin, were relatively well preserved as illustrated in Figure 1.

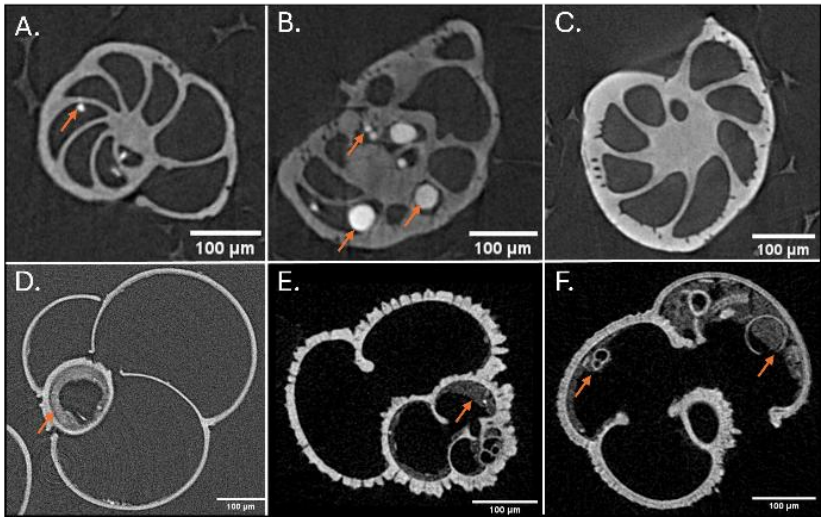

Figure 1. Sources of variability in µCT scans of foraminifera. Orange arrows highlight heterogeneous fine and coarse grain sediment infill within foraminifera chambers, illustrating differences in infill spatial density across specimens. Additional variation in image contrast is also evident between samples. Panels A–C show benthic species, while panels D–F show planktonic species.

Parameter	Unit	Description	Measurements reported in previous studies
Calcite volume	μm^3	Total volume of the test, excluding the chamber volumes.	(Kuroyanagi et al. 2021; Kinoshita et al. 2022; Zarkogiannis et al. 2025; Burke et al. 2020)
Test volume	μm^3	Test volume including chamber volumes.	(Zarkogiannis et al. 2019; Kinoshita et al. 2021)
Surface area	μm^2	Surface area of filled calcite 3D volume.	(Belanger 2022)
Internal chamber volume	μm^3	Volume of internal chambers, summed.	(Burke et al. 2020; Speijer et al. 2008; Burke et al. 2025; Duan et al. 2021; Briguglio et al. 2011)
Chamber centroid	Coordinates, x y and z.	X-Y-Z coordinates of each chamber.	(Lin et al. 2024)
Inner septa thickness	μm^3	Average thickness of the inner test septa	(Johnstone et al. 2010; François et al. 2022; Iwasaki et al. 2019)
Outer test thickness	μm^3	Average thickness of the outer test wall	(Iwasaki et al. 2019; Fox et al. 2020; Ni et al. 2025)

Table 1: Table of parameters incorporated within ForamJ.

Installation and download

For local Fiji installation download the ZIP file for your OS from imagej.net/software/fiji/downloads, extract the folder (e.g., Fiji.app), and run the executable. Prior to running ForamJ from the ImageJ interface, the following plugins must also be installed: BoneJ (Doube et al. 2010), 3D imageJ Suite (Ollion et al. 2013), IJ-plugins (Sacha 2016) and Morphology (Legland et al. 2016). For plugins, use Help > Update within Fiji to manage update sites or manually drag JAR/class files into the Fiji.app/plugins/ folder and restart Fiji. Following download of the .ijm file from the supplementary information of this article, it must be dropped into the plugins folder of the local Fiji installation. ForamJ will be maintained on the corresponding authors GitHub, at the url: https://github.com/JTrendFiji/ForamJ. All method development was completed in Fiji ver 2.16.0.

Methodological workflow

Image stacks (of greyscale .tif or .tiff files) are processed using a custom ImageJ macro designed to support both Single Image and Batch modes. The processing workflow executed by this plugin is schematically presented in Figure 2. In Single Image mode, the user selects a single .tif file for manual processing (Figure 2.1). In Batch mode, all .tif or .tiff files within a selected directory are processed automatically (Figure 2.2). For both single and batch mode, ForamJ analyses one individual specimen per scan, akin to those produced by Searle-Barnes et al. (2025), whereby each field of view contained only a single specimen. Should the user scan multiple samples within a singular field of view, specimens should be separated first, into separate datasets, with one sample per tiff stack.

For each dataset, the macro creates two output directories: one for image outputs (Sample_Images) and one for tabulated results (Sample_Results), where Sample refers to the base filename). No known naming rules apply here, although we recommend avoiding characters that are invalid or problematic in file systems (such as /, \, :, *, ?, ", <, >, |). Voxel dimensions in the X, Y, and Z directions (µm) are specified by the user to ensure spatial accuracy (Figure 2.3). An optional infill removal step is included, in which users inspect the image stack and, if necessary, apply a manual threshold to generate an infill mask (Figure 2.4). This mask is subtracted from the original dataset using image arithmetic, yielding a cleaned volume referred to as the Raw image.

Segmentation of the foraminiferal test begins by duplicating the Raw volume and applying a 3D Gaussian blur to reduce image noise, followed by thresholding defined by the user (Figure 2.5). A "keep-largest-region" operation is used to eliminate non-target debris, and a morphological closing sequence (3D dilation, hole filling, erosion) generates a filled outer mask (FilledMask) representing the complete test morphology (Figure 2.6). Here, the user is asked to confirm whether the test is completely filled. If yes, then the user moves onto the next step. If not – and some inner chambers are not infilled - the user directs the use of a 3D Euclidean Distance Transform (EDT) to infill the inner chambers (Figure 2.7).

Specifically, a distance map is created from the filled calcite ROI, and the user then choses a threshold which seals off chambers which have remained open, followed by a second EDT which is overlaid onto the binary skeleton image, with the user then once again selecting a threshold to infill the remaining test, ensuring that the threshold does not spill over into, as to not artificially augment the test size. Once complete, this image is renamed to replace the previous filled outer mask. An approximation of surface area is computed from the FilledMask by identifying edge voxels and multiplying their count by the average voxel face area based on the user-defined voxel dimensions. This metric is exported as a CSV.

To delineate septal and outer wall structures, a 3D Euclidean Distance Transform (EDT) is applied to the FilledMask. Users then threshold the EDT to isolate the septal region (Figure 2.8), and the outer test and internal septa are exported as individual binary masks. A 3D thickness analysis (BoneJ plugin) is performed on each, yielding thickness maps and summary statistics.Subtracting the initial skeleton from the FilledMask produces a binary representation of the internal chamber volume (InnerChambers). For chamber segmentation, the InnerChambers volume is smoothed with a 3D Gaussian filter, and an EDT is applied. Users then generate seed regions via binary thresholding, ensuring chambers are spatially distinct. These seeds are labelled using 3D connected components analysis and passed to a 3D watershed algorithm, enabling segmentation of discrete chambers even when septal walls are partially degraded (Figure 2.9). Each chamber's centroid, volume, and average intensity are extracted and saved.

The plugin also computes total volumes for the SkeletonBinary, FilledMask, and InnerChambers masks by summing voxel counts and scaling by voxel volume. These values, along with all intermediate and final masks (e.g., distance maps, watershed labels, thickness maps), are saved as .tif images and .csv files for reproducibility and downstream analysis (Figure 2.10). At each manual thresholding step, users are prompted to enter the applied minimum and maximum threshold values, which are logged in a ProcessingLog.txt file for traceability.

Image Outputs

For each processed image stack, the macro generates a set of standardised image outputs, saved in the Sample_Images directory (where *Sample* refers to the base filename of the input image). These include both intermediate and final masks used in morphological and volumetric analyses. The core outputs are:

- **Raw.tif** – the greyscale input image (post-infill removal, if applied).
- **SkeletonBinary.tif** – a binary mask representing the thresholded skeletal test.
- **FilledMask.tif** – a binary mask of the test after morphological closure.
- **InnerChambers.tif** – internal chamber space, derived by subtracting the skeletal mask from the filled test.
- **InnerTest.tif** – a binary mask of the internal septal region.
- **InnerTestThicknessMap.tif** – 3D thickness map of the inner test.
- **OuterTest.tif** – a binary mask of the outer test (test wall).
- **OuterTestThicknessMap.tif** – 3D thickness map of the outer test.
- **EdgeVoxelsForSA.tif** – binary edge mask used for surface area estimation.
- **WatershedLabels.tif** – segmented chamber stack, generated via 3D watershed.

If infill removal is enabled, an additional image (Infill.tif) is saved, containing the user-defined infill mask. Additional supporting images include DistanceMap.tif (Euclidean Distance Transform), SeedImage.tif (thresholded seed regions), and LabeledSeeds.tif (connected components of seed points), all used in chamber segmentation. All outputs are exported in .tif format using a consistent naming scheme for traceability.

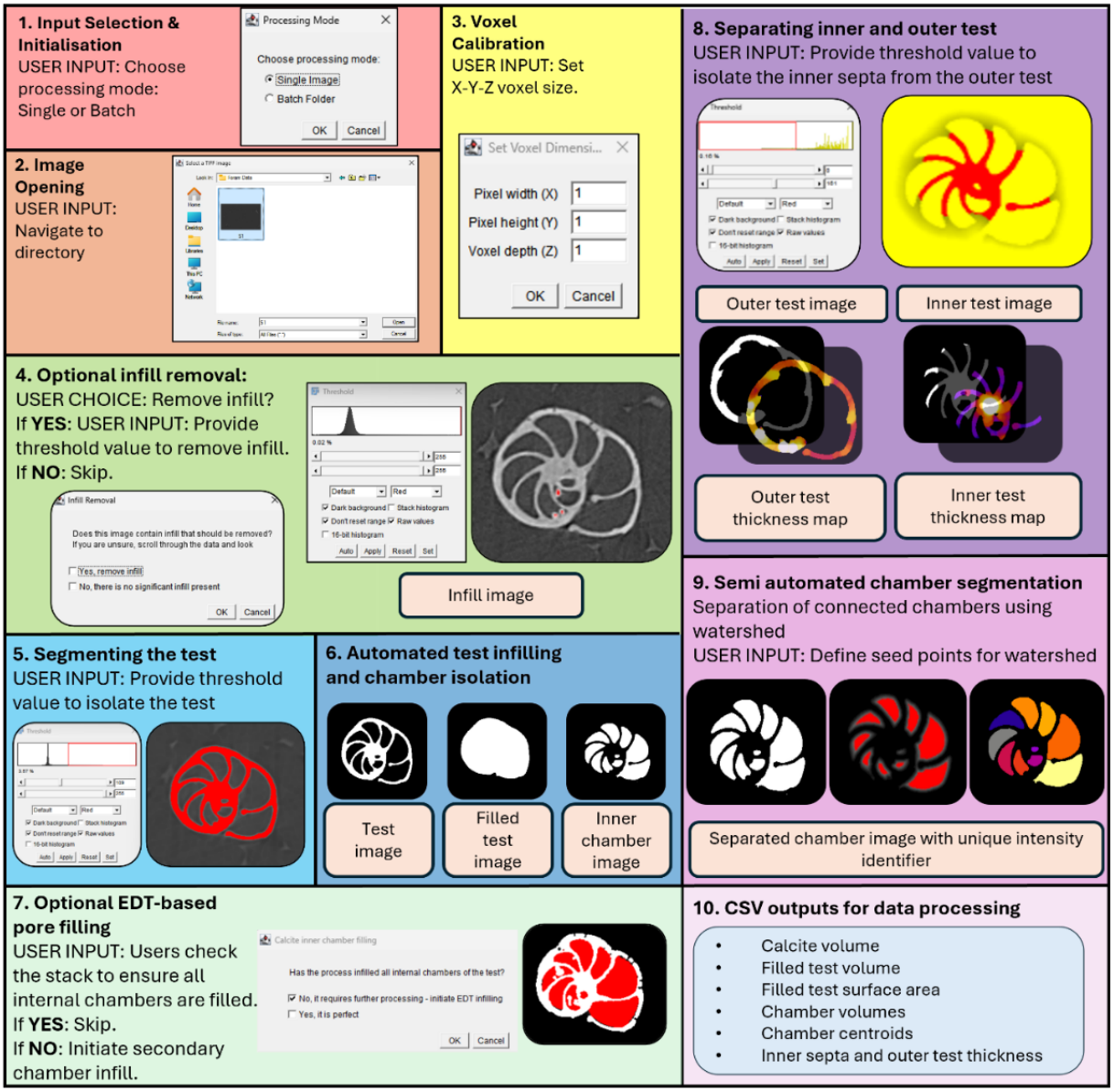

Figure 2 – ForamJ workflow for segmentation and morphometric analysis of foraminiferal µCT datasets. The procedure begins with (1) input selection (single image or batch) and (2) file opening, followed by (3) voxel calibration to set X–Y–Z dimensions. (4) Optional infill removal allows users to exclude artificial material prior to analysis. (5) Thresholding isolates the test from background, leading to (6) automated chamber infilling and chamber mask generation. (7) An optional EDT-based pore filling step ensures internal chambers are completely closed. (8) Threshold-based separation of the inner septa from the outer test produces (9) thickness maps and enables semi-automated chamber segmentation using watershed with user-defined seed points. (10) The workflow outputs multiple CSV files containing quantitative descriptors including calcite volume, filled test volume, surface area, chamber volumes, centroids, chamber counts, and septal thickness.

Quantification Outputs

The macro generates several .csv files summarising morphometric and structural properties, saved in the Sample_Results directory. These include:

- Sample_StructureVolumes.csv: Total volumes (in voxels and µm³) for three key structures:
- *SkeletonBinary*: Representing the calcite shell as a binary image.
- *FilledMask*: The total test volume, with inner chambers filled.
- *InnerChambers*: Internal chamber space: Volume is calculated by counting binary voxels and scaling by the user-defined voxel volume.
- *Sample_FilledMask_SurfaceArea.csv*: An estimate of surface area is computed by detecting edge voxels in the *FilledMask* volume and multiplying the total edge voxel count by the average voxel face area (accounting for anisotropic voxel dimensions).
- *Sample_OuterTestThickness.csv and Sample_InnerTestThickness.csv*: Mean and distributional thickness metrics for both outer and inner test regions, computed using the BoneJ particle analysis module.
- *Sample_ChamberVolumes.csv, Sample_ChamberCentroids.csv, and Sample_ChamberIntensities.csv, combined into a CombinedChamberDetail.csv,* acting as a series of quantitative outputs derived from the *WatershedLabels* image. These include: Individual chamber volumes, 3D centroid coordinates and Mean voxel intensities (using *WatershedLabels* as both object and signal image).

At each manual segmentation step, users are prompted to input the minimum and maximum threshold values used. These values, along with voxel dimensions and key processing decisions (e.g. all threshold values that are used), are saved in a plain-text log file: Sample_ProcessingLog.txt. This log ensures transparency and supports reproducibility across datasets. The time taken to process the sample is also logged.

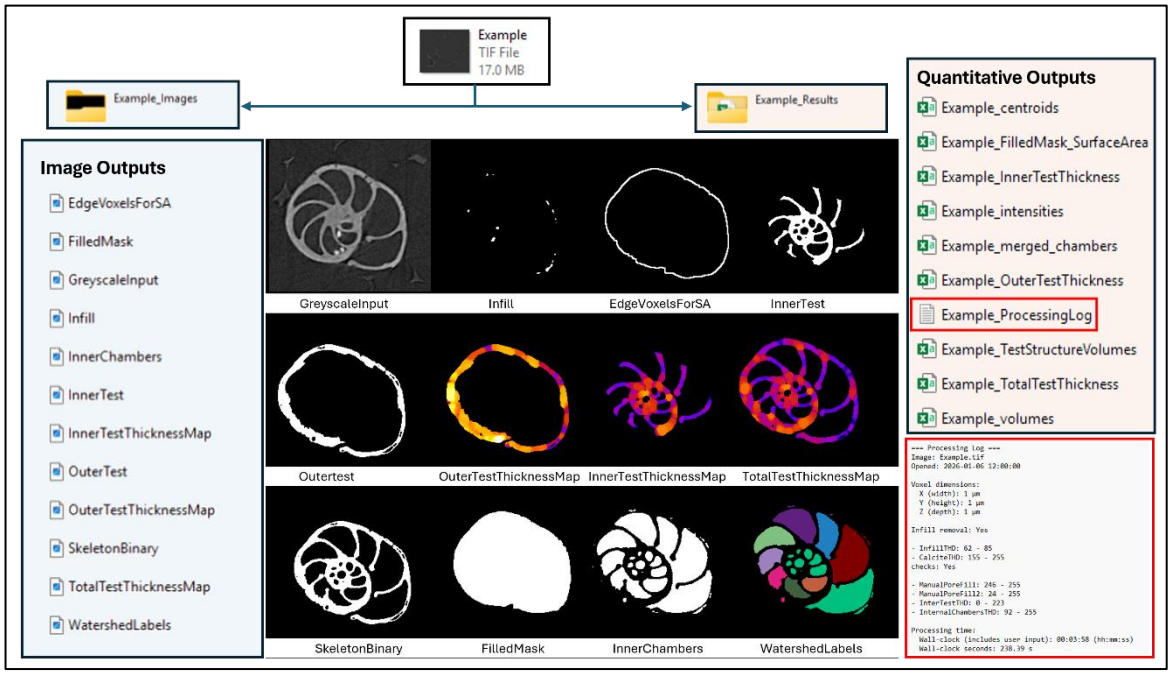

Figure 3 – ForamJ Output format

Processing in ForamJ generates a series of image outputs (listed left, shown centre), quantitative outputs (right, listed) and a log output (right, lower).

Statistical analysis

The use of single samples for comparisons of benthic foraminifera is reported in text as a mean value. Meanwhile reporting of duplicates per species of planktonic foraminifera were accompanied by the reporting of both values or a mean value. All graphs were made in GraphPad Prism (ver 10.4.1).

Application 1 – study of benthic foraminifera

Seven samples (Table 2) were scanned at the University of Southampton, muvis X-Ray imaging centre. Benthic foraminifera recovered from deep-sea core sites can exhibit varying degrees of shell dissolution due to exposure to chemically corrosive bottom waters and porewaters following burial (Corliss and Honjo 1981). In contrast, clay-rich lithologies from continental shelf environments often yield exceptionally well-preserved foraminiferal specimens with glassy or translucent shell textures that are well suited for µCT image analysis (Pearson et al. 2001). Fossil benthic foraminiferal species *Cibicidoides alleni* (Plummer 1926) and *Cibicidoides succedens* (Brotzen 1970) were selected from Eocene age sediments (~56 million years ago) obtained from the Ocean Drilling Program (ODP) Leg 174AX Bass River core, located in present-day New Jersey, USA (Miller et al. 1998). The paleo-environment of Bass River makes it a preferred location for image analysis because it was a continental shelf setting, well above the depths of potentially chemical corrosive deep waters and it contains high clay content that acts as an impermeable to limit fluid interaction and post depositional dissolution. A range of benthic foraminiferal sizes were selected for assessment to maximize the ranges in parameters (Table 1). While the *Cibicidoides* benthic foraminiferal shells are well-preserved chemical cleaning was conducted to minimise potential surficial contamination prior to image analysis. Whole marine sediment samples were disaggregated in Milli-Q water (18.2 Ω) using an orbital shaker and wet sieved to separate the coarse sand fraction > 63 µm for microfossil selection. Benthic foraminifera specimens were analysed from a narrow range of multiple size fractions 180–212, 212–250 and 250–300 µm and among sample depths spanning the entire PETM section to maximise the potential morphological variability in the sample set. Individual benthic foraminifera were placed in the centre of a watch glass under a stereomicroscope to be chemical cleaned prior to µCT analysis. The chemical cleaning protocol included sequential ethanol and Milli-Q water (18.2 Ω) rinses (3-5 times each) to remove adhered clay and sediments from the outside surface of the foraminiferal shell. Due to the variable solution viscosities, both ethanol and Milli-Q are utilized during cleaning to better facilitate surficial particle removal from the porous foraminiferal wall texture. Cleaned individuals were mounted into straws between evenly spaced layers of varying porosity foam to aid in mapping out target analyses and distinguish sample sets prior to scanning, as described (Searle-Barnes et al. 2025).

µCT scanning was completed in collaboration with muvis x-ray imaging centre, using a Zeiss Versa 610 x-Ray imaging system. Once mounted, high-resolution µCT scans were acquired using 110 kV, 10 W, with 1001 projections collected over 360°. An exposure time of 1.3s was used with a low-energy x-ray filter, yielding a total scan duration of 53 minutes per sample, 2x binning was used to provide a voxel size of 1.75 µm.

SpecimenID	Species	Depth of sample (m)	Size of sample (µm)	Research group	Voxel size (µm)
1145_180_CS3	*Cibicidoides succedens*	1145.00	180	Case Western Reserve University	1.75
1145_212_CS0	*Cibicidoides succedens*	1145.00	212	Case Western Reserve University	1.75
1145_250_CS0	*Cibicidoides succedens*	1145.00	250	Case Western Reserve University	1.75
11583_212_CS1	*Cibicidoides succedens*	1583.00	212	Case Western Reserve University	1.75
11583_250_CS0	*Cibicidoides succedens*	1583.00	250	Case Western Reserve University	1.75
1159_180_CA0	*Cibicidoides alleni*	1159	180	Case Western Reserve University	1.75
1159_250_CA0	*Cibicidoides alleni*	1159.00	250	Case Western Reserve University	1.75

Table 2: Benthic foraminifera sample information.

For validation of the segmentation achieved by ForamJ, authors completed a similar workflow in Dragonfly 2024.1 relying on manual segmentation for the separation of infill, calcite and background. Authors chose to utilise the commercial software Dragonfly as the gold standard for segmentation and analysis. Utility of the 3D painter tool governed this, as a faster alternative to manual segmentation in Fiji. The segmentation for the calcite volume (Figure 4A) was then compared as a volume versus the ForamJ output. Across all examined benthic foraminifera, there was a 1.30% difference in calcite volume between ForamJ and Dragonfly. Use of the segmentation comparison tool facilitated calculation of segmentation accuracy (0.9981 ± 0.001), Dice score (0.97 ± 0.008), True Negative Rate (0.9972 ± 0.001), and True Positive Rate (0.9781 ± 0.016) suggestive that ForamJ reproduced manual segmentation faithfully (Figure 4B). Comparison of manual segmentation and ForamJ-derived segmentation may be observed in Figures 4 C-F.

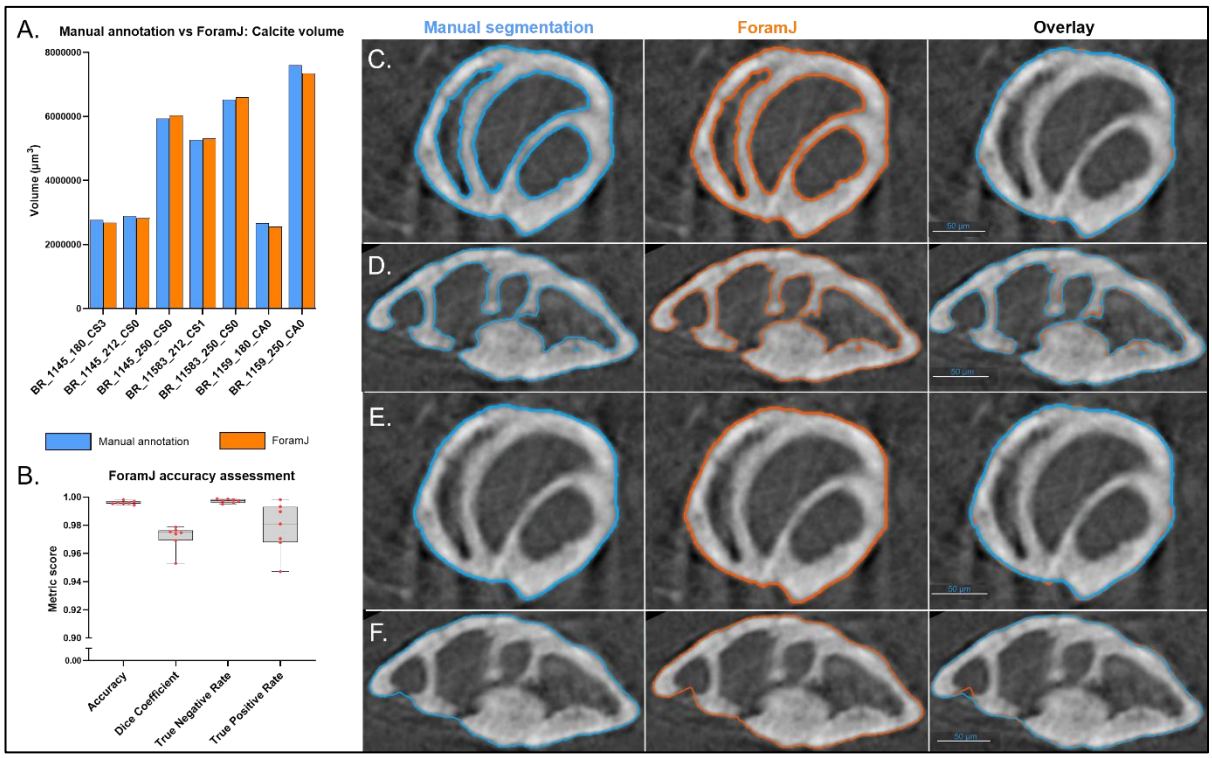

Figure 4 – ForamJ validation.
Processing of benthic foraminifera tests in Dragonfly (blue) and ForamJ (orange) for the comparative segmentation of calcite volume (A), and other comparative metrics, including accuracy, Dice score, true negative rate and true positive rate (B). (C-F) Show the comparative segmentation from the two methods, with the left hand column showing the manual segmentation result, right hand panel showing the ForamJ result (C) and (D) show this segmentation of the calcite volume, while (E) and (F) show the segmentation of the test volume.

Subsequent morphometric analyses completed by ForamJ revealed clear inter-specimen variability in test architecture (Figure 5). Calcite volumes ranged from 2.6×10^6 µm³ (BR_1159_180_CA0) to over 6.6×10^6 µm³ (BR_11583_250_CSO), broadly reflecting differences in test size. Test porosity spanned 26.7–49.7%, with most specimens clustering between 39–44%. Wall thickness ranged from 31.2 µm in BR_1145_212_CS0 to 56.9 µm in BR_1159_180_CA0, with inner septa consistently thinner than outer test walls. Test surface areas varied between ~5.7×10^5 µm² and >1.2×10^6 µm², while chamber volumes produced distinct growth trajectories: BR_1145_250_CSO, with 25 chambers, exhibited the steepest cumulative increase, in contrast to the smaller, more compact form of BR_1145_212_CS0 (9 chambers). Together, these measurements highlight marked differences in skeletal investment and chamber organisation across specimens.

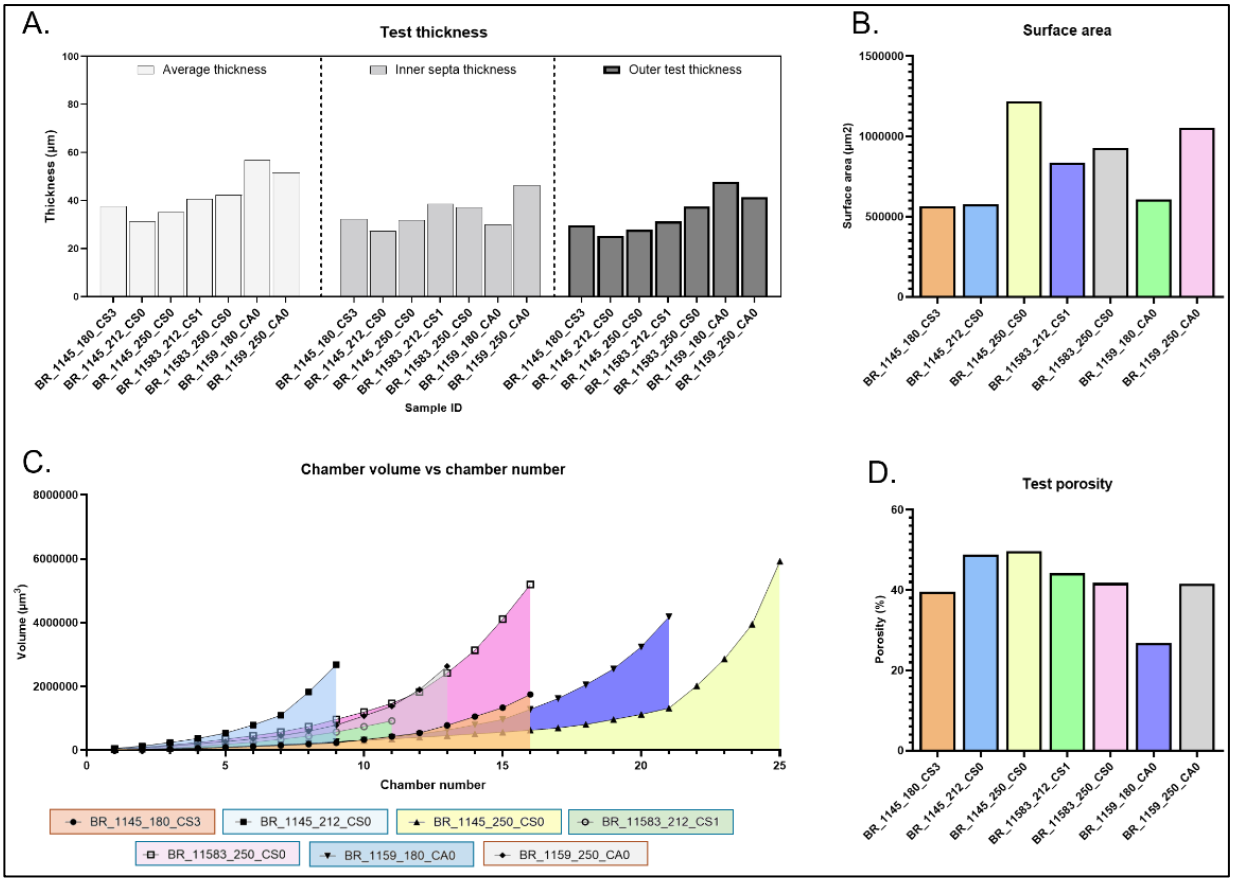

Figure 5 – Quantitative morphometric measurements derived from µCT-based segmentation of benthic foraminiferal tests.

ForamJ was used to segment µCT scans for the assessment of benthic foraminifer, yielding several morphometric measurements. (A) Test wall thickness measurements separated into average thickness (light grey), inner septa thickness (mid grey), and outer test thickness (dark grey) across multiple specimens. (B) Calculated test surface areas (µm²) for each specimen. (C) Chamber-by-chamber volumetric growth curves, showing the relationship between chamber number and chamber volume (µm³), with shaded regions highlighting specimen-specific trajectories. (D) Test porosity (%) calculated as the ratio of chamber volume to total test volume. Data is shown as mean values.

Application 2: ForamJ for the study of planktonic foraminifera

To showcase the utility of ForamJ to the wider foraminifera community, two individuals from seven planktonic foraminifera species were processed using ForamJ, accessed from the repository provided by (Siccha et al. 2023) summarised in Table 3. This application was used to showcase the variety of test morphologies that could be assessed using ForamJ. The µCT image collection of planktonic foraminifera compiled by Siccha et al. (2023) represents a unique benchmark dataset in the micropaleontological research community, by providing an optimal resource for developing image processing techniques. This is primarily because it is open access and secondly because the images are supplied as raw greyscale files without prior segmentation or processing which is important in the light of foraminiferal µCT processing being laboratory-specific and lacking a standardised reference sample set. Moreover, the taxonomy of all planktonic foraminifera specimens has been independently validated and are curated, enabling follow-up investigations and repeat measurements when necessary. Collectively, for these factors make the dataset exceptionally well-suited for future inter-comparative studies, as it allows for consistent re-evaluation of µCT analyses.

µCT-derived morphometric analyses revealed pronounced interspecific differences in test architecture among the examined planktonic foraminifera (Figure 5), including calcite volume (Figure 6A), test volume (Figure 6B), porosity (Figure 6C), surface area (Figure 6D), wall thickness (Figure 6E), and chamber volume trajectories (Figure 6F).

SpecimenID	Species (Genus species)	Sample method	Station / Campaign	Lat	Lon	Research group	Voxel size (µm)
CA_CNI_1	*Candeina nitida*	Sediment	GeoB3935-1 / M49/2	12.613	−59.388	Bordeaux	1.2004
CA_CNI_2	*Candeina nitida*	Sediment	GeoB3935-1 / M49/2	12.613	−59.388	Bordeaux	1.2004
GE_TSA_5	*Trilobatus sacculifer*	Sediment	GeoB3803-1 / M34/3	−30.048	−8.572	JAMSTEC	1.0003
GE_TSA_6	*Trilobatus sacculifer*	Sediment	GeoB3803-1 / M34/3	−30.048	−8.572	JAMSTEC	1.0003
IC_DAN_1	*Dentigloborotalia anfracta*	Plankton tow	SO226/K276	171.587	-34.533	Bordeaux	1.2016
IC_DAN_2	*Dentigloborotalia anfracta*	Plankton tow	M140_985-1	-28.745	15.867	MAPEX Bremen	0.3741
RO_GSC_1	*Globorotalia scitula*	Plankton tow	SO226 / K276	171.587	-34.533	Bordeaux	1.1986
RO_GSC_2	*Globorotalia scitula*	Plankton tow	M140 / GeoB22408-1	-30.377	11.867	MAPEX Bremen	0.3639
GE_GBU_8	*Globigerina bulloides*	Sediment	GeoB3803-1 / M34/3	−30.048	−8.572	JAMSTEC	1.0003
GE_GBU_9	*Globigerina bulloides*	Sediment	GeoB3803-1 / M34/3	−30.048	−8.572	JAMSTEC	1.0003
RO_GIN_12	*Globorotalia inflata*	Sediment	GeoB1210-3 / M12/1	−24.485	7.438	JAMSTEC	1.0003
RO_GIN_13	*Globorotalia inflata*	Sediment	GeoB1210-3 / M12/1	−24.485	7.438	JAMSTEC	1.0003
GE_GEL_3	*Globigerinoides elongatus*	Sediment	GeoB3803-1 / M34/3	−30.048	−8.572	JAMSTEC	1.0003
GE_GEL_4	*Globigerinoides elongatus*	Sediment	GeoB1210-3 / M12/1	−24.485	7.438	JAMSTEC	1.0003

Table 3: Planktonic foraminifera sample information.

Candeina nitida (CA_CNI) species displayed the highest porosities (85.4%, 87.7%), combined with the thinnest walls, with inner septal thicknesses of 12.0 µm and 12.9 µm and outer wall thicknesses of 28.5 µm and 29.7 µm. Despite their delicate structure, chamber volumes reached 4.8 × 10^7 µm³ and 5.0 × 10^7 µm³, supported by calcite volumes of 6.8 × 10^6 µm³ and 8.6 × 10^6 µm³. Growth trajectories were relatively linear, reflecting steady volumetric expansion (Figure 6G). *Globigerina bulloides* (GE_GBU) species exhibited substantially thicker walls, with inner septa of 26.4 µm and 34.4 µm and outer walls of 42.3 µm and 42.7 µm, alongside lower porosities (62.1%, 69.5%). Individual chambers frequently exceeded 9.6 × 10^6 µm³, contributing to total test volumes of 1.5 × 10^8 µm³ and 1.6 × 10^8 µm³, supported by calcite volumes of 4.7 × 10^6 µm³ and 5.9 × 10^6 µm³. Chamber growth was stepwise, with disproportionately large additions during the outer whorl (Figure 6H). *Globigerinoides elongatus* (GE_GEL) species combined moderate porosities (57.4%, 71.7%) with inner septal thicknesses of 36.7 µm and 42.9 µm and outer wall thicknesses of 39.3 µm and 54.6 µm. Chamber volumes reached 1.6 × 10^7 µm³, with calcite volumes of 6.3 × 10^6 µm³ and 6.7 × 10^6 µm³, and cumulative growth curves showed marked late-stage expansion (Figure 6I). Similarly, *Trilobatus sacculifer* (GE_TSA) exhibited porosities of 56.9% and 57.4%, with inner septa of 40.1 µm and 47.5 µm and outer walls of 50.1 µm and 54.5 µm. Chamber volumes were 1.2 × 10^7 µm³ and 1.4 × 10^7 µm³, supported by calcite volumes of 7.1 × 10^6 µm³ and 7.8 × 10^6 µm³. *Dentigloborotalia anfracta* (IC_DAN) showed higher variability, with porosities of 60.2% and 80.4%, inner septa of 29.3 µm and 36.7 µm, and outer walls of 25.7 µm and 36.2 µm. Chamber volumes were comparatively small (7.7 × 10^6 µm³, 9.6 × 10^6 µm³), and calcite volumes limited (2.0 × 10^6 µm³, 4.6 × 10^6 µm³), resulting in shallow cumulative growth profiles (Figure 6K).

Globorotalia inflata (RO_GIN) exhibited intermediate porosities (60.7%, 79.3%) with inner septa of 30.4 µm and 34.8 µm and outer walls of 32.5 µm and 36.7 µm. Chamber volumes reached 1.1 × 10^7 µm³ and 1.4 × 10^7 µm³, supported by calcite volumes of 5.2 × 10^6 µm³ and 5.8 × 10^6 µm³, with steady volumetric increases across successive chambers (Figure 6L). By contrast, *Globorotalia scitula* (RO_GSC) produced compact tests with porosities of 72.5% and 73.1%, inner septa of 17.3 µm and 21.3 µm, and outer walls of 25.7 µm and 36.2 µm. Chamber volumes were 3.6 × 10^6 µm³ and 1.1 × 10^7 µm³, supported by calcite volumes of 1.4 × 10^6 µm³ and 5.0 × 10^6 µm³. Surface areas were comparatively high (2.3 × 10^6 µm², 2.6 × 10^6 µm²), reflecting greater external complexity despite reduced volumetric growth.

Together, these data demonstrate a continuum of test morphologies, ranging from thin-walled, highly porous tests with rapid chamber proliferation *Candeina nitida* (CA_CNI) to thick-walled, low-porosity taxa with thicker test architectures consistent with a greater proportion of gametogenic calcite (Bé 1980). *Trilobatus sacculifer* (GE_GBU), with other species occupying intermediate positions defined by moderate porosity, chamber expansion, and wall thickness.

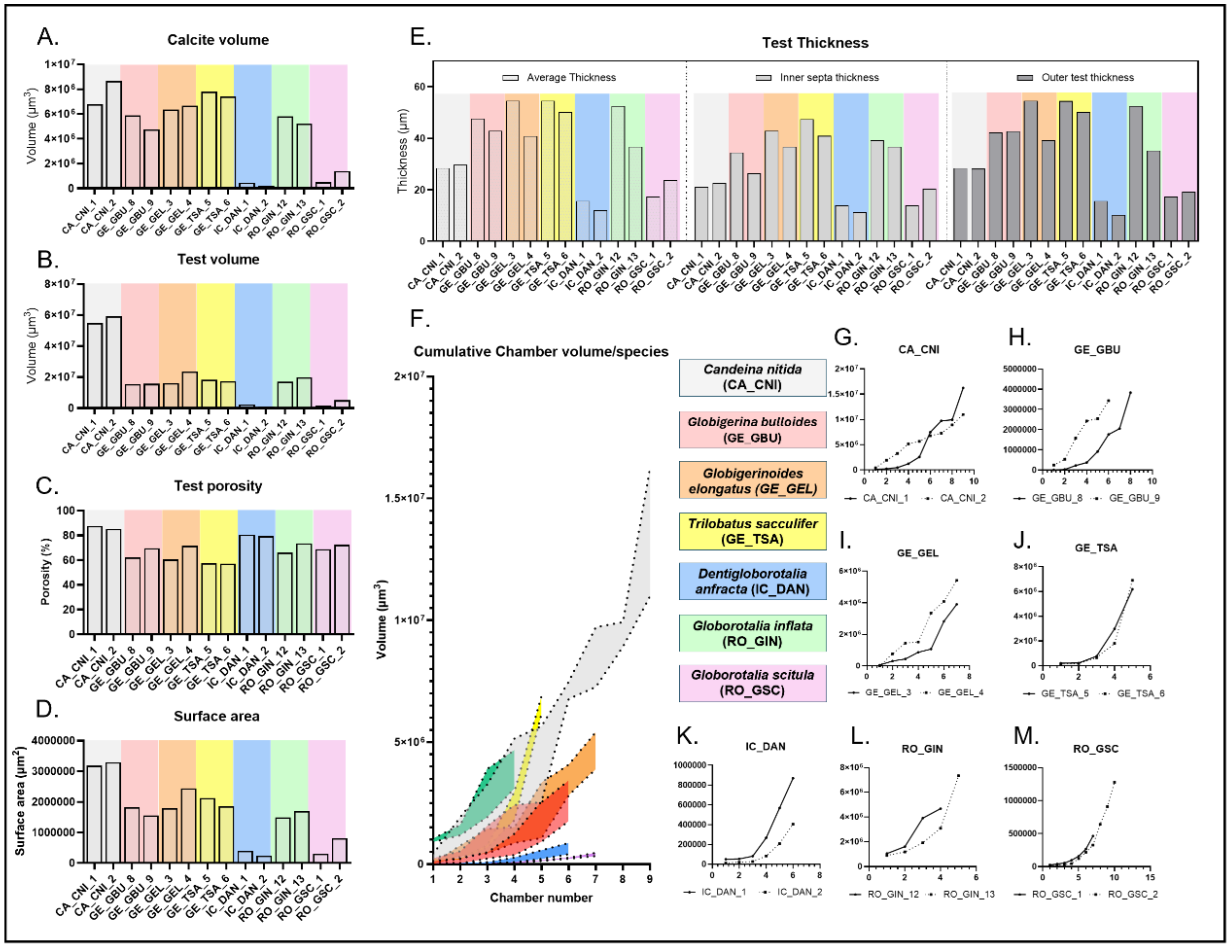

Figure 6. Inter-species comparison of test architecture in planktonic foraminifera using ForamJ. Quantitative morphometric traits were extracted from 3D reconstructions of multiple species to assess variation in test architecture for the assessment of multiple species of planktonic foraminifera: (A) Calcite volume, (B) total test volume, (C) porosity, and (D) surface area measured across species. (E) Test thickness metrics separated into average, inner septa, and outer test thickness. (F) Cumulative chamber volume curves show species-level growth trajectories with data shown as mean ± SD per species. (G–M) Displays the chamber-by-chamber growth curves for individual species, highlighting similarities between individuals of the same species.

Throughput and portability

All processing on applications 1 and 2 were completed on a non-specialist laptop, equipped with 8GB of RAM. Datasets used varied across two orders of magnitude; with the speed of processing varying significantly as a function of dataset size (Figure 7). The smallest dataset (RO_GSC_1) was 14 MB and took 78 seconds to process, while the largest dataset (RO_GSC_2) was 940 MB and took 782 seconds to process. The median dataset size was 142 MB, with a processing speed of 154 seconds. Processing of these datasets on a relatively low-capacity workstation highlights ForamJ's portability even for the processing of larger (~1 GB) datasets.

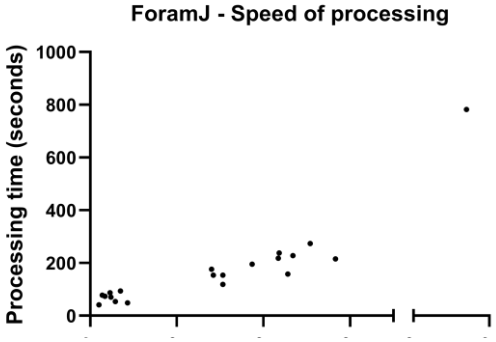

Figure 7: ForamJ processing speed. Dataset size (MB) is plotted against processing time (seconds), showcasing the scalable relationship even on low-capacity workstations.

Discussion

ForamJ provides several advantages over existing software; it provides a number of metrics that are defined by the need within the existing literature. It does so in open source, non-commercial software, allowing for a one stop use experience for the analysis of µCT datasets of foraminifera, with applications to both benthic and planktonic foraminifera.

Importantly, it addresses a number of limitations of existing software. Namely, it is contained within the open-source environment of Fiji-ImageJ rather than relying on specialist, costly, commercial software. ForamJ meanwhile provides a user-friendly user walkthrough of processing alongside an easy, lightweight setup, allowing non-specialist users to complete morphological analyses.

The workflow also acts to improve on throughput, by providing an optional “Single” or “Batch” mode. This “Single” mode allows for the user to test and validate the workflow versus existing methods, while the batch mode allows the user to move through high sample numbers. Additionally, the uniform export of tiff stacks allows for the user to combine ForamJ with their own downstream analysis pipelines.

ForamJ also attempts to circumvent the potential for non-homogenous µCT scans, should greyscale values vary between or within sessions or scanners. The use of a manual thresholding step allows the user to control this element of segmentation, without requiring a complex segmentation approach, utilising complex workflows, machine learning or even deep learning algorithms. While this approach has also been used to reduce infill contamination, it is noted that this is primarily designed for the removal of discrete infilling (i.e. siliciclastic), and that more complex infill removal may be facilitate by dedicated segmentation plugins such as WEKA (Arganda-Carreras et al. 2017) or more advanced cleaning protocols prior to imaging. Additionally, while integration within the open-source Fiji environment provides a number of advantages, allowing for the prioritisation of throughput, quantification and reproducibility, it does possess limited 3D rendering versus commercial software such as ORS Dragonfly, Aviso/Amira, VG Studio and IPSDK. Currently, ForamJ does not prioritise this 3D rendering, although opening of an image stack output and rendering using the 3D Viewer plugin, does allow for this need to be met in some capacity and does provide an exciting angle for future releases.

Similarly, the desire to isolate pores within the test itself, is a need that is currently unmet by ForamJ. Pores within the test are often poorly resolved and will require the development of further segmentation-focused modules, which the authors anticipate being added to ForamJ in future updates and releases. On this note, users may request and provide feedback to ForamJ using the email address ForamJDevs@gmail.com. While ForamJ is provided as a freely available software, the responsibility of validating individual results lies with the user, not the developer.

Acknowledgements

For programming advice, we thank the ImageJ community, especially Dr David Chatalet, Dr Alisha Sharma, and Dr Simon Lane. Professor Gavin Foster, Professor Thomas Ezard, Dr James Mulqueeny and Dr. Sargent Bray at the University of Southampton for providing lab support and discussions of methodological design and data acquisition. CWRU undergraduate student Jasmine Shah for assistance with benthic foraminifera selection and µCT analysis. We thank (Siccha et al. 2023) for the data used in Application 2, and muvis X-Ray imaging centre for the scans acquired in Application 1.

The authors acknowledge the µ-VIS X-ray Imaging Centre at the University of Southampton for the provision of the X-ray tomographic imaging facilities. The Zeiss Versa 610 used within this research was upgraded by EPSRC Core equipment 2024, grant UKRI391 and was originally purchased via ‘Southampton Imaging: 3D imaging at millimetre to nanometre scales for regenerative medicine using multiple complimentary modalities’ through MRC grant MR/L012626/1.

Author contributions

Study design: JT, TB. Data collection: JT, FB. Data analysis JT. Data interpretation: JT Drafting manuscript: JT, FB, TB.

Funding

Financial support for the study through NERC-NSF GEO CFORCE NE/W009625/1 and Case Western Reserve University faculty startup funds awarded to TLB.

Data availability statement

Datasets showcased for applications (1) and (2) are publicly available. For application (1), data is accessible in the supplementary material of this article, while (2) is freely available by (Siccha et al. 2023), using the following URL: https://doi.pangaea.de/10.1594/PANGAEA.949585.

Conflict of interest statement

The authors declare that there is no conflict of interest.

References

Arganda-Carreras, Ignacio, Verena Kaynig, Curtis Rueden, et al. 2017. 'Trainable Weka Segmentation: A Machine Learning Tool for Microscopy Pixel Classification'. *Bioinformatics (Oxford, England)* 33 (15): 2424–26. https://doi.org/10.1093/bioinformatics/btx180.

Arshadi, Cameron, Ulrik Günther, Mark Eddison, Kyle I. S. Harrington, and Tiago A. Ferreira. 2021. 'SNT: A Unifying Toolbox for Quantification of Neuronal Anatomy'. *Nature Methods* 18 (4): 374–77. https://doi.org/10.1038/s41592-021-01105-7.

Barker, Chris, Darren Naish, Jacob Trend, et al. 2023. 'Modified Skulls but Conservative Brains? The Palaeoneurology and Endocranial Anatomy of Baryonychine Dinosaurs (Theropoda: Spinosauridae)'. *Journal of Anatomy* 242 (February). https://doi.org/10.1111/joa.13837.

Bé, A. W. H. 1980. 'Gametogenic Calcification in a Spinose Planktonic Foraminifer, *Globigerinoides Sacculifer* (Brady)'. *Marine Micropaleontology* 5 (January): 283–310. https://doi.org/10.1016/0377-8398(80)90014-6.

Belanger, Christina L. 2022. 'Volumetric Analysis of Benthic Foraminifera: Intraspecific Test Size and Growth Patterns Related to Embryonic Size and Food Resources'. *Marine Micropaleontology* 176 (September): 102170. https://doi.org/10.1016/j.marmicro.2022.102170.

Briguglio, ANTONINO, BRIAN METSCHER, and JOHANN HOHENEGGER. 2011. 'Growth Rate Biometric Quantification by X-Ray Microtomography on Larger Benthic Foraminifera: Three-Dimensional Measurements Push Nummulitids into the Fourth Dimension'. *Turkish Journal of Earth Sciences* 20 (6): 683–99. https://doi.org/10.3906/yer-0910-44.

Brombacher, Anieke, Alex Searle-Barnes, Wenshu Zhang, and Thomas H. G. Ezard. 2022. 'Analysing Planktonic Foraminiferal Growth in Three Dimensions with foram3D: An R Package for Automated Trait Measurements from CT Scans'. *Journal of Micropalaeontology* 41 (2): 149–64. https://doi.org/10.5194/jm-41-149-2022.

Brotzen, Fritz. 1970. *The Swedish Paleocene and Its Foraminiferal Fauna*. Sveriges Geologiska Undersökning. Antiquariaat Junk. https://cir.nii.ac.jp/crid/1971149384741805481.

Burke, Janet E., Leanne E. Elder, Amy E. Maas, et al. 2025. 'Physiological and Morphological Scaling Enables Gigantism in Pelagic Protists'. *Limnology and Oceanography* 70 (2): 461–76. https://doi.org/10.1002/lno.12770.

Burke, Janet E., Willem Renema, Ralf Schiebel, and Pincelli M. Hull. 2020. 'Three-Dimensional Analysis of Inter-and Intraspecific Variation in Ontogenetic Growth Trajectories of Planktonic Foraminifera'. *Marine Micropaleontology* 155 (March): 101794. https://doi.org/10.1016/j.marmicro.2019.101794.

Cnudde, V., and M. N. Boone. 2013. 'High-Resolution X-Ray Computed Tomography in Geosciences: A Review of the Current Technology and Applications'. *Earth-Science Reviews* 123 (August): 1–17. https://doi.org/10.1016/j.earscirev.2013.04.003.

Corliss, Bruce H., and Susumu Honjo. 1981. 'Dissolution of Deep-Sea Benthonic Foraminifera'. *Micropaleontology* 27 (4): 356–78. https://doi.org/10.2307/1485191.

Doube, Michael, Michał M Kłosowski, Ignacio Arganda-Carreras, et al. 2010. 'BoneJ: Free and Extensible Bone Image Analysis in ImageJ'. *Bone* 47 (6): 1076–79. https://doi.org/10.1016/j.bone.2010.08.023.

Duan, Baichuan, Tiegang Li, and Paul N. Pearson. 2021. 'Three Dimensional Analysis of Ontogenetic Variation in Fossil Globorotaliiform Planktic Foraminiferal Tests and Its Implications for Ecology, Life Processes and Functional Morphology'. *Marine Micropaleontology* 165 (May): 101989. https://doi.org/10.1016/j.marmicro.2021.101989.

Evans, Holly, Rebecca Andrews, Fatma Abedi, et al. 2024. 'Evidence for Peri-Lacunar Remodeling and Altered Osteocyte Lacuno-Canalicular Network in Mouse Models of Myeloma-Induced Bone Disease'. *JBMR Plus* 8 (July). https://doi.org/10.1093/jbmrpl/ziae093.

Fox, Lyndsey, Stephen Stukins, Thomas Hill, and C. Giles Miller. 2020. 'Quantifying the Effect of Anthropogenic Climate Change on Calcifying Plankton'. *Scientific Reports* 10 (1): 1620. https://doi.org/10.1038/s41598-020-58501-w.

François, Daniel, Adina Paytan, Olga Maria Oliveira de Araújo, Ricardo Tadeu Lopes, and Cátia Fernandes Barbosa. 2022. 'Acidification Impacts and Acclimation Potential of Caribbean Benthic Foraminifera Assemblages in Naturally Discharging Low-pH Water'. *Biogeosciences* 19 (22): 5269–85. https://doi.org/10.5194/bg-19-5269-2022.

He, Yichen, Marco Camaiti, Lucy E. Roberts, et al. 2025. 'SPROUT: A User-Friendly, Scalable Toolkit for Multi-Class Segmentation of Volumetric Images'. Preprint, bioRxiv, August 14. https://doi.org/10.1101/2024.11.22.624847.

Isensee, Fabian, Maximilian Rokuss, Lars Krämer, et al. 2025. 'nnInteractive: Redefining 3D Promptable Segmentation'. arXiv:2503.08373. Preprint, arXiv, March 11. https://doi.org/10.48550/arXiv.2503.08373.

Iwasaki, S., K. Kimoto, Y. Okazaki, and M. Ikehara. 2019. 'Micro-CT Scanning of Tests of Three Planktic Foraminiferal Species to Clarify DissolutionProcess and Progress'. *Geochemistry, Geophysics, Geosystems* 20 (12): 6051–65. https://doi.org/10.1029/2019GC008456.

Johnstone, Heather J. H., Michael Schulz, Stephen Barker, and Henry Elderfield. 2010. 'Inside Story: An X-Ray Computed Tomography Method for Assessing Dissolution in the Tests of Planktonic Foraminifera'. *Marine Micropaleontology* 77 (1): 58–70. https://doi.org/10.1016/j.marmicro.2010.07.004.

Judd, Emily J., Jessica E. Tierney, Brian T. Huber, et al. 2022. 'The PhanSST Global Database of Phanerozoic Sea Surface Temperature Proxy Data'. *Scientific Data* 9 (1): 753. https://doi.org/10.1038/s41597-022-01826-0.

Katz, Miriam E., Benjamin S. Cramer, Allison Franzese, et al. 2010. ‘TRADITIONAL AND EMERGING GEOCHEMICAL PROXIES IN FORAMINIFERA’. *Journal of Foraminiferal Research* 40 (2): 165–92. https://doi.org/10.2113/gsjfr.40.2.165.

Kinoshita, Shunichi, Azumi Kuroyanagi, Hodaka Kawahata, et al. 2021. ‘Temperature Effects on the Shell Growth of a Larger Benthic Foraminifer (*Sorites Orbiculus*): Results from Culture Experiments and Micro X-Ray Computed Tomography’. *Marine Micropaleontology* 163 (March): 101960. https://doi.org/10.1016/j.marmicro.2021.101960.

Kinoshita, Shunichi, Quan Wang, Azumi Kuroyanagi, Masafumi Murayama, Yurika Ujiié, and Hodaka Kawahata. 2022. ‘Response of Planktic Foraminiferal Shells to Ocean Acidification and Global Warming Assessed Using Micro-X-Ray Computed Tomography’. *Paleontological Research* 26 (4): 390–404. https://doi.org/10.2517/PR200043.

Kucera, Michal, Mara Weinelt, Thorsten Kiefer, et al. 2005. ‘Reconstruction of Sea-Surface Temperatures from Assemblages of Planktonic Foraminifera: Multi-Technique Approach Based on Geographically Constrained Calibration Data Sets and Its Application to Glacial Atlantic and Pacific Oceans’. *Quaternary Science Reviews*, Multiproxy Approach for the Reconstruction of the Glacial Ocean surface, vol. 24 (7): 951–98. https://doi.org/10.1016/j.quascirev.2004.07.014.

Kuroyanagi, Azumi, Takahiro Irie, Shunichi Kinoshita, et al. 2021. ‘Decrease in Volume and Density of Foraminiferal Shells with Progressing Ocean Acidification’. *Scientific Reports* 11 (1): 19988. https://doi.org/10.1038/s41598-021-99427-1.

Legland, David, Ignacio Arganda-Carreras, and Philippe Andrey. 2016. ‘MorphoLibJ: Integrated Library and Plugins for Mathematical Morphology with ImageJ’. *Bioinformatics* 32 (22): 3532–34. https://doi.org/10.1093/bioinformatics/btw413.

Lin, Huahua, Wenshu Zhang, James Mulqueeney, et al. 2024. ‘3DKMI: A MATLAB Package to Generate Shape Signatures from Krawtchouk Moments and an Application to Species Delimitation in Planktonic Foraminifera’. *Methods in Ecology and Evolution* 15 (September): 1940–48. https://doi.org/10.1111/2041-210X.14388.

Ma, Jun, Yuting He, Feifei Li, Lin Han, Chenyu You, and Bo Wang. 2024. ‘Segment Anything in Medical Images’. *Nature Communications* 15 (1): 654. https://doi.org/10.1038/s41467-024-44824-z.

Meijering, E., M. Jacob, J.-C.f. Sarria, P. Steiner, H. Hirling, and M. Unser. 2004. ‘Design and Validation of a Tool for Neurite Tracing and Analysis in Fluorescence Microscopy Images’. *Cytometry Part A* 58A (2): 167–76. https://doi.org/10.1002/cyto.a.20022.

Miller, K.G., P.J. Sugarman, J.V. Browning, and et al., eds. 1998. *Proceedings of the Ocean Drilling Program, 174AX Initial Reports*. Vol. 174A. Proceedings of the Ocean Drilling Program. Ocean Drilling Program. https://doi.org/10.2973/odp.proc.ir.174AX.1998.

Moore, Brad T., James M. Jordan, and L. Ryan Baugh. 2013. ‘WormSizer: High-Throughput Analysis of Nematode Size and Shape’. *PloS One* 8 (2): e57142. https://doi.org/10.1371/journal.pone.0057142.

Mulqueeney, James M., Alex Searle-Barnes, Anieke Brombacher, Marisa Sweeney, Anjali Goswami, and Thomas H. G. Ezard. 2024. ‘How Many Specimens Make a Sufficient Training Set for Automated Three-Dimensional Feature Extraction?’ *Royal Society Open Science* 11 (6): rsos.240113. https://doi.org/10.1098/rsos.240113.

Ni, Sha, Dirk Müter, Laurie M. Charrieau, et al. 2025. ‘Morphological Insights From Benthic Foraminifera for Environmental Conditions in the Baltic Sea During the Last Interglacial’. *Paleoceanography and Paleoclimatology* 40 (3): e2024PA005063. https://doi.org/10.1029/2024PA005063.

Ollion, Jean, Julien Cochennec, François Loll, Christophe Escudé, and Thomas Boudier. 2013. ‘TANGO: A Generic Tool for High-Throughput 3D Image Analysis for Studying Nuclear Organization’. *Bioinformatics* 29 (14): 1840–41. https://doi.org/10.1093/bioinformatics/btt276.

Papazoglou, Andreas S., Efstratios Karagiannidis, Dimitrios V. Moysidis, et al. 2021. ‘Current Clinical Applications and Potential Perspective of Micro-Computed Tomography in Cardiovascular Imaging: A Systematic Scoping Review’. *Hellenic Journal of Cardiology* 62 (6): 399–407. https://doi.org/10.1016/j.hjc.2021.04.006.

Pearson, Paul N., Peter W. Ditchfield, Joyce Singano, et al. 2001. ‘Warm Tropical Sea Surface Temperatures in the Late Cretaceous and Eocene Epochs’. *Nature* 413 (6855): 481–87. https://doi.org/10.1038/35097000.

Plummer, Helen Jeanne. 1926. *Foraminifera of the Midway Formation in Texas*. The University.

Sacha, Jarek. (2016) 2016. *Ij-Plugins/Ijp-Toolkit*. Java. March 30; IJ-Plugins, released. https://github.com/ij-plugins/ijp-toolkit.

Schindelin, Johannes, Ignacio Arganda-Carreras, Erwin Frise, et al. 2012. ‘Fiji: An Open-Source Platform for Biological-Image Analysis’. *Nature Methods* 9 (7): 676–82. https://doi.org/10.1038/nmeth.2019.

Searle-Barnes, Alex, Anieke Brombacher, Orestis Katsamenis, Kathryn Rankin, Mark Mavrogordato, and Thomas Ezard. 2025. ‘Ten Recommendations for Scanning Foraminifera by X-Ray Computed Tomography’. *Journal of Micropalaeontology* 44 (1): 107–17. https://doi.org/10.5194/jm-44-107-2025.

Siccha, Michael, Raphael Morard, Julie Meilland, Shinya Iwasaki, Michal Kucera, and Katsunori Kimoto. 2023. ‘Collection of X-Ray Micro Computed Tomography Images of Shells of Planktic Foraminifera with Curated Taxonomy’. PANGAEA. https://doi.org/10.1594/PANGAEA.949585.

Speijer, Robert P., Denis Van Loo, Bert Masschaele, Jelle Vlassenbroeck, Veerle Cnudde, and Patric Jacobs. 2008. ‘Quantifying Foraminiferal Growth with High-Resolution X-Ray Computed Tomography: New Opportunities in Foraminiferal Ontogeny, Phylogeny, and Paleoceanographic Applications’. *Geosphere* 4 (4): 760–63. https://doi.org/10.1130/GES00176.1.

Trend, Jacob, Alisha Sharma, Lysanne Michels, et al. 2023. ‘Regional Assessment of Male Murine Bone Exposes Spatial Heterogeneity in Osteocyte Lacunar Volume Associated with Intracortical Canals and Regulation by VEGF | bioRxiv’. Preprint, bioRxiv. https://www.biorxiv.org/content/10.1101/2023.02.08.527672v2.

Westerhold, Thomas, Norbert Marwan, Anna Joy Drury, et al. 2020. ‘An Astronomically Dated Record of Earth’s Climate and Its Predictability over the Last 66 Million Years’. *Science* 369 (6509): 1383–87. https://doi.org/10.1126/science.aba6853.

Withers, Philip, Charles Bouman, Simone Carmignato, et al. 2021. ‘X-Ray Computed Tomography’. *Nature Reviews Methods Primers*, ahead of print, February 25. https://doi.org/10.1038/s43586-021-00015-4.

Zarkogiannis, Stergios D., Assimina Antonarakou, Aradhna Tripati, et al. 2019. ‘Influence of Surface Ocean Density on Planktonic Foraminifera Calcification’. *Scientific Reports* 9 (1): 533. https://doi.org/10.1038/s41598-018-36935-7.

Zarkogiannis, Stergios D., James W. B. Rae, Benjamin R. Shipley, and P. Graham Mortyn. 2025. ‘Planktonic Foraminifera Regulate Calcification According to Ocean Density’. *Communications Earth & Environment* 6 (1): 605. https://doi.org/10.1038/s43247-025-02558-w.